Submit an article   Journal homepage

[�))) Listen] [▶]

🔓 Open access

Articles

VIIRS night-time lights

Christopher D Elvidge ✉, **Kimberly Baugh**,
Mikhail Zhizhin, **Feng Chi Hsu** & **Tilottama Ghosh**

❝ Download citation
🔗 https://doi.org/10.1080/01431161.2017.1342050

[Check for updates]

➕

ABSTRACT

The Visible Infrared Imaging Radiometer Suite
(VIIRS) Day/Night Band (DNB) collects global
low-light imaging data that have significant

improvements over comparable data collected for 40 years by the DMSP Operational Linescan System. One of the prominent features of DNB data is the detection of electric lighting present on the Earth's surface. Most of these lights are from human settlements. VIIRS collects source data that could be used to generate monthly and annual science grade global radiance maps of human settlements with electric lighting. There are a substantial number of steps involved in producing a product that has been cleaned to exclude background noise, solar and lunar contamination, data degraded by cloud cover, and features unrelated to electric lighting (e.g. fires, flares, volcanoes). This article describes the algorithms developed for the production of high-quality global VIIRS night-time lights. There is a broad base of science users for VIIRS night-time lights products, ranging from land-use scientists, urban geographers, ecologists, carbon modellers,

📄 Full Article   🖼 Figures & data   📑 References   66 Citations 🔺

📊 Metrics   © Licensing   🖨 Reprints & Permissions   PDF

In this article ✖

‹ **Previous** article   **View** issue table of contents   **Next** article ›

Related articles ℹ

People also read   Recommended articles

1. Introduction

Global satellite-observed night-time lights have emerged as one of the widely used geospatial data products (Amaral et al. 2005; Small, Pozzi, and Elvidge 2005; Sutton et al. 2007; Bharti et al. 2009; Chand et al. 2009; Ghosh et al. 2010; Oda and Maksyutov 2011; Witmer and O'loughlin 2011; He et al. 2012; Mazor et al. 2013; Min et al. 2013; Falchi et al. 2016). These products show the locations where artificial lighting is present and a measure of the brightness as observed from space. From 1992 to 2013, there is a consistently processed annual time series of night-time lights processed from low-light imaging data collected by the US Air Force Defense Meteorological Satellite Program (DMSP) Operational Linescan System (OLS) (Baugh et al. 2010). The follow on to DMSP for global low-light imaging of the Earth at night is the Visible Infrared Imaging Radiometer Suite (VIIRS) Day/Night Band (DNB), flown jointly by NASA and NOAA. The VIIRS DNB provides several key improvements over DMSP-OLS data, including a vast reduction in the pixel footprint (ground instantaneous field of view [GIFOV]), uniform GIFOV from nadir to edge of scan, lower detection limits, wider dynamic range, finer quantization, and in-flight calibration (Miller et al. 2012; Elvidge et al. 2013;

Remote sensing of night-time light ›

Xi Li et al.
International Journal of Remote Sensing
Published online: 24 Jul 2017

Evaluation of NPP-VIIRS night-time light composite data for extracting built-up urban areas ›
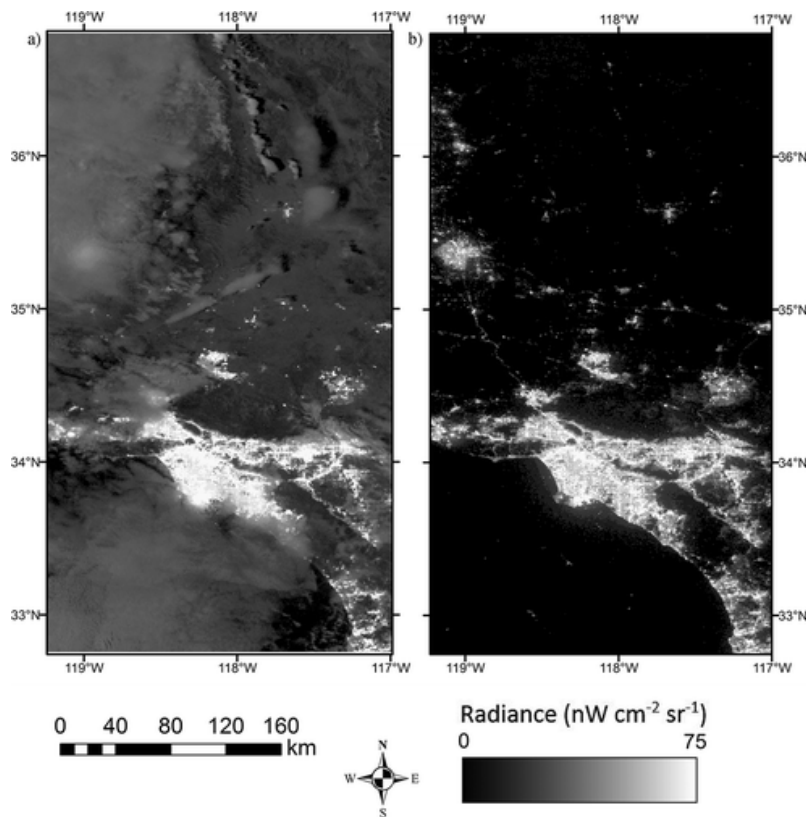
Kaifang Shi et al.
Remote Sensing Letters
Published online: 14 Apr 2014

Responses of Suomi-NPP VIIRS-derived nighttime lights to

Miller et al. 2013).

The fundamental purpose of both DMSP and VIIRS low-light imaging is to enable the detection of clouds using moonlight instead of sunlight as the illumination source. The requirement for this capability comes from meteorologists. However, a broad swath of natural and social sciences accrues benefits from the unintended ability of these systems to detect lighting at the Earth's surface. On a heavily moonlit night, the DNB images look like daytime images with clouds and Earth's surface features clearly visible (Figure 1(a)). The telltale sign that the image was acquired at night is the city lights present on the land surface. Under new moon conditions, the outlines of clouds and land surface features are suppressed (Figure 1(b)). However, close inspection of moonless night-time DNB data reveals the dim outline of high albedo clouds and land surface features. This remarkable capability has been linked to nocturnal airglow (Min et al. 2013). In addition, the DNB records several other types of phenomena unrelated to electric lighting, including stray light, lightning, biomass burning, gas flares, high energy particle (HEP) detections, atmospheric glow surrounding bright sources, and background noise.

Figure 1. Full moon *versus* new moon VIIRS Day/Night Band (DNB) data for the Los Angeles region. (a) Full moon data. (b) New moon data.

Display full size

To produce a night-time lights product, the low-light imaging data need to be filtered to exclude low-quality data and extraneous features through a cascading series of filtering steps prior to temporal averaging. The resulting average radiance product has null values (zero) in areas where surface lighting was not detected. Until recently, there has not been a night-time lights product available from VIIRS.

The first version of a VIIRS night-time lights product is now available at https://www.ngdc.noaa.gov/eog/viirs.html. In this article, we describe the methods developed by NOAA to produce DNB night-time lights.

2. Methods

The procedures for generating VIIRS night-time lights involve a series of filtering steps to exclude the various styles of extraneous features (Table 1) followed by an averaging of the radiance values. Five styles of global grids are generated at 15 as resolution. This grid cell size is slightly finer that the 742-m DNB pixel footprints. The coverage (CVG) grid tallies the number of observations during the year that were free of sunlight, moonlight, straylight, and HEP detections. The cloud-free coverage (CF_CVG) grid tallies the number of CVG observations that were also cloud-free. Three varieties of DNB radiance grids are produced. The first DNB grid is a raw cloud-free composite (RCFC), with sunlit, moonlit, stray light, lightning, HEP filtering, and cloud filtering. This product contains lighting features, plus biomass burning, aurora, gas flares, volcanoes, and

background noise. The second DNB grid is an outlier-removed cloud-free composite (ORCFC), with biomass burning and portions of the aurora are removed. The third DNB grid is VIIRS Nighttime Lights (VNL), with full filtering of all the noted extraneous features removed except lights from persistent gas flares. Below is a description of the filters and processing steps.

Table 1. Filter types and thresholds used to exclude non-lighting grid cells.

CSV   Display Table

2.1. Sunlit data

Sunlit data are removed by discarding pixels having solar zenith angles less than 101°. At solar zenith angles above 101°, the Sun is well below the horizon and the conditions on the ground are fully free from the effects of solar illumination. Solar zenith angles are provided for each pixel from the DNB geolocation file. It should be noted that eliminating sunlit data results in high latitude black outs surrounding the summer solstice. During these periods, significant portions of the high latitude zones

have extremely low numbers of dark night observations. Over a full year, it is possible to fill these gaps and make a usable product spanning 65°S–75°N.

2.2. Moonlit data

A lunar illumination (LI) threshold of 0.0005 lx and below is used for screening moonlit data. LI is calculated based on the per cent of LI, lunar zenith, and azimuth using a model from the US Navy (Janiczek and Deyoung 1987). The model inputs (latitude, longitude, date, and time) are extracted from DNB geolocation file.

2.3. Stray light data

The VIIRS DNB radiances are contaminated by stray light when the spacecraft is illuminated by sunlight while observing the areas of the Earth's surface where the sun is under the horizon. Stray light occurs at mid-to-high latitudes and the affected zone reaches its maximum latitudinal extent at the summer solstice. While there is a stray light correction (Mills, Weiss, and Liang 2013), the correction leaves residual features that would propagate into the annual product. To avoid inclusion of potentially under-or-over corrected data, we exclude stray light contaminated data from the annual

composites.

2.4. HEP detections

Two methods are used to filter out HEP detections. An initial filtering is done using thresholds placed on the DNB radiance and spike height index (SHI) (Elvidge et al. 2015). SHI is calculated in two stages. First, by computing the relative difference between the pixel's radiance and the average of the two adjacent pixels. This calculation is done for the two adjacent pixels in the same scan line (or row), and then for the two adjacent pixels in the same sample position (or column). The final SHI is the min of these two intermediate values. Pixels with SHI values greater than .995 that also have radiance values greater than 1000 nW are filtered out. This eliminates the brightest of the HEP detections. Additional HEP detections are filtered out via the outlier removal procedure described in Section 2.7.

2.5. Lightning

Because DNB data are collected 16 lines at a time, lightning detections create a characteristic 16-line horizontal stripe. Each 16-line sweep across the Earth is termed a scan. A method was developed in 2014 to detect and filter out

lightning (Elvidge et al. 2015). The procedure involves calculating the relative radiance difference between adjacent lines of DNB data. The analysis is only done for pairs of lines forming the edges of the 16-line scans. A threshold of 10% is placed on the log-scaled relative radiance difference. When the number of adjacent pixels passing the threshold exceeds 24, the scan segment on the higher radiance side is labelled as lightning. This eliminates most of the lightning from affecting the composites, but some very weak lightning can remain which is filtered out via the outlier removal procedure described in Section 2.7.

2.6. Cloud screening

Clouds tend to obscure and scatter the radiance from lighting. Opaque clouds can fully block the observation of lighting. Thinner clouds reduce the observed radiance and scatter the light, creating a fuzzy appearance. We use the VIIRS cloud mask (VCM) (Godin and Vicente 2015) to screen out pixels deemed to be clouds. Kopp et al. (2014) analysed the accuracy of the VCM and report that the night-time VCM has an 86.4% accuracy, with 4.4% false alarms and 7.3% missed clouds.

2.7. Outlier removal

The primary purpose of the outlier removal is to exclude pixels with biomass burning, which are expressed as anomalously high radiance pixels but occur infrequently over an entire year. The high side outlier removal has the additional benefit of filtering out some of the aurora affected pixels. Filtering out the low radiance outliers has a more subtle effect on the average, by filtering out observations that may be affected by clouds (errors in the cloud mask) or power outages.

We adapted the outlier removal algorithm developed for DMSP-OLS night-time lights (Baugh et al. 2010) to work on the DNB data. The outlier removal is conducted on histograms generated for each of the 15 as grid cells in the composite. Due to the large dynamic range of the DNB, a logarithmic scaling is done on the radiance values used in the RCFC to transform the individual pixel radiances from nW to log-scaled radiance (LSR) values ranging from 0 to 255. First, a constant of 2 is added to the DNB values so that the logarithm is not applied to negative numbers. LSR values greater than 255 are forced to 255.

The outlier removal algorithm excludes pixels

one at a time from the high and low end of the histogram. After each removal, the standard deviation is recomputed and compared to the standard deviation before that pixel removal. The outlier removal stops when the standard deviation stabilizes by changing either less than 1%, or by 0.075 (Figure 2). Following outlier removal, the LSRs for the remaining pixels are averaged to generate a log-scaled ORCFC.

Figure 2. Outlier removal is applied to each 15 as grid cell. This histogram of 2015 data is for the grid cell at (10.43125 N, 1.31875 W) in Ghana, Africa.

Display full size

2.8. Defining the local background

Background is the residual radiance in areas that lack detectable surface lighting. In general, background radiances are quite small, with the vast majority under 1 nW. However, there are sufficient variations in background that it is impossible to set a single threshold to separate lights from background. There is also a noticeable rise in background, termed glow, that surrounds large cities and gas flares.

We developed a three-step process for defining local background. In the first step, we use an image texture measure known as data range. The data range is a convolution filter, calculated for each grid cell using a kernel size of 3, or the three-by-three block of surrounding cells. The data range for the centre pixel is calculated as the maximum LSR minus the minimum in the kernel. An example, covering a portion of Myanmar is shown in Figure 3(a,b). The initial pixel set for use in defining the background pixel set is selected using the data range and CF_CVG grids. The data range threshold rises as CF_CVGs decline (Figure 4) to accommodate the higher variability present in regions having low numbers of CF_CVGs. The data range is low in areas with no surface lighting.

Figure 3. Two key grids used to define background pixel sets: (a) Data range calculated using a 3 × 3 kernel. Background areas have low data ranges; (b) lambda1 is used to define small dim lighting features over land that are excluded from the background pixel set.

Display full size

Figure 4. The threshold used to select the initial

background pixel set rises as the number of cloud-free observations decreases. Thresholds are log-scaled radiance values.

Display full size

From this initial background pixel set, we remove remaining small faint light sources on land based on a concavity measure known as lambda1. Lambda1 is computed from the log-scaled ORCFC image and is the smallest magnitude eigenvalue of the Hessian matrix (Frangi et al. 1998; Lindeberg 1998). Lambda1 will be negative in areas where the log-scaled ORCFC image is concave down, which occurs in the centre of small lighting features. Lambda 1 values less than −0.55 were removed from the background pixel set over land only (Figure 3). The result is a global grid of background radiances with null values (zeros) in grid cells with lighting or adjacent to lighting (Figure 5(a)). We refer to this pixel set as the background seeds. The third step is to fill the null values with the radiance of the nearest background grid cell (Figure 5(b)).

Figure 5. The final steps in defining the background: (a) After defining the seeds

background pixel set, the average radiances are restored from the outlier-removed cloud-free composite, leaving zeros in the areas with data ranges that are above the selection threshold or lambda1 values over land less than −0.55; (b) the holes are filled using the radiance from the nearest background pixel. Note that the effects of glow surrounding bright lights can be seen in both the seeds grid and the background grid. The seeds grid contains part of the glow adjacent to bright lighting. The glow pixels are subsequently propagated to fill the holes in the background grid.

Display full size

2.9. Defining areas with surface lighting

The next step is to define areas with surface lighting by subtracting the ORCFC LSR and the log-scaled background radiance. A delta of 0.8 is added to the background to trim off some of the glow that surrounds lighting. This threshold was derived empirically based on visual inspection of difference values in the glow surrounding large cities where no indication of surface lighting was evident. Positive values in

the difference image indicate the presence of surface lighting.

2.10. Manual editing

After subtracting the background radiance from the ORCFC, several types of non-lighting features are set to zero using hand drawn masks. This includes grid cells affected by aurora, high mountain tops, volcanoes, and grid cells surrounding extremely low CF_CVG zones, with numbers of cloud-free observations less than 2.

2.11. Restoring the radiance values

The difference image created by subtracting the local background works quite well for identifying areas with surface lighting. However, close inspection reveals that the boundaries between regions filled by different seed radiances propagate into the difference. While we are interested to develop a radiance product with a background correction, the current method of filling the holes in the seeds image will need to be improved for this. For this reason, the ORCFC radiance is restored for all grid cells determined to have surface lighting to produce the night-time lights product (VNL).

2.12. Identification of gas flares

Ideally, gas flares and the glow surrounding gas flares would be filtered out of the night-time lights product leaving only electric lighting sources. While small gas flares have no obvious glow, large gas flares have spatially extensive glow which starts out with high radiance values and declines with distance out from the source. An algorithm for filtering out the glow surrounding gas flares is under development. In the meantime, a gas flaring vector set is available, with more than 12,000 flaring sites identified in 2015. The identification of flaring sites is based on annual composites of VIIRS nightfire (Elvidge et al. 2016) temperatures and detection frequencies. Flaring sites are indicated for grid cells with average temperature exceeding 1200 K and per cent detection frequencies of 1% or more.

3. Results

A total of five global grids are produced as a VIIRS night-time lights suite. The global grids are huge, 86,400 grid cells wide and 33,600 high. This exceeds the size limitation for the standard geotiff format, so the global grids are cut into six tiles. The first grid tallies the

number of usable CVGs or observations that pass through the primary filtering to remove pixels contaminated by sunlight, moonlight, stray light, lightning, and HEP (Figure 6). The histogram (Figure 7) of the CVG image shows that 0.003% of grid cells have zero CVGs and 97% of the grids cells have more than 100 CVGs in 2015. The histogram shows a series of peaks and troughs that appear to be latitude related variations in the usable CVGs.

Figure 6. Grid tallying the number of usable coverages (CVG) for 2015. The tally includes pixels that passed filtering steps for sunlight, moonlight, stray light, and HEP detections.

Display full size

Figure 7. Histogram of coverage tallies for 2015.

Display full size

The second grid, referred to as CF_CVG, tallies the number of CVG pixels that passed the cloud filter (Figure 8). The histogram of the CF-CVG grid (Figure 9) indicates that 99% of grid cells had 20 or more CF_CVGs and only 0.003% had zero CF_CVGs. This indicates that outside of a

few low CVG areas, the vast majority of areas have sufficient numbers of cloud-free observations to generate a high-quality night-time lights product.

Figure 8. Grid tallying the number of cloud-free coverages (CF_CVG) for 2015. The tally includes the CVG pixels minus those pixels deemed to be cloudy by the VIIRS cloud mask.

Display full size

Figure 9. Histogram of the cloud-free coverages for 2015.

Display full size

Visual inspection indicates that the overall background rises as latitude increases. This was also the case for the DMSP night-time lights. Figure 10 shows the average background radiance as a function of latitude. The average background varies from −0.05 to 1.075 nW, a range of approximately 1 nW. The background is lowest between 50°S and 50°N, with average radiances under 0.2 nW. The average background radiance drops slightly below zero between 10°S and 50°S latitude. This is

attributed to the use of northern hemisphere dark night ocean data in establishing the dark current level for night-time DNB calibration. The background then rises in two stages from 51° to 65°S, probably due to the influence of the aurora Australis. The background rises rapidly from 50°N to 70°N and then drops at about the same rate out to 75°N. The rise and fall of the background north of 50° is believed to be a reflection of auroral activity.

Figure 10. Average background radiance as a function of latitude for 2015.

Display full size

Three varieties of annual VIIRS DNB cloud-free composites were produced for 2015. Examples of the three are shown in Figures 11(a–c). The first is the RCFC, which retains biomass burning, aurora, and background. The second is the ORCFC, with biomass burning and portions of the aurora filtered out. The third composite, night-time lights (VNL), is generated by removing background from the ORCFC. The data for the three are floating point values and the units are average radiances in nW cm^{-2} sr^{-1}.

Figure 11. Three styles of VIIRS DNB average

radiance grids were produced for 2015: (a) the raw cloud-free composite (RCFC), which has lights, biomass burning, and aurora present; (b) the outlier-removed cloud-free composite (ORCFC) that has been filtered to remove fires and some aurora; (c) night-time lights (VNL) with the background and all extraneous features removed except gas flaring.

Display full size

Figure 12 shows a log-scaled histogram of the distribution of radiance present in the VIIRS night-time lights. The histogram peaks at 1.4 nW with more than 1.3 million grid cells per bin. The numbers fall off rapidly as radiance increases and at the extreme high end, the numbers of grid cells per bin drop to single digits. Above 13,000 nW, the number of grid cells per bin is under 10, and above 22,000 nW, there are one or two grid cells per bin. Las Vegas, Nevada peaks out at 2800 nW, leaving 1475 grid cells brighter than Las Vegas. It is believed that the majority of these are gas flares. Below 1.4 nW, the number of grid cells per bin also drops precipitously to 14,000 grid cells at 1 nW. This decline is likely an expression of the VIIRS DNB detection limits.

Figure 12. Histogram of the 2015 VIIRS night-time lights. There are vastly larger numbers of low radiance grid cells *versus* high radiance cells.

Display full size

We wanted to determine whether population centres were being removed from the VNL product as a result of outlier and background removal. Our procedures intentionally seek to remove biomass burning and the glow that surrounds urban centres. To investigate the effectiveness of the outlier and background removal, we extracted Landscan 2015 (Bright, Rose, and Urban 2016) population counts for three varieties of background. Australia was selected for the analysis because it has annual biomass burning and vast areas having scant population.

The first background set consists of the grid cells where the average of high end outliers was 5 nW or greater. These are grid cells with biomass burning activity. The remaining background grid cells were divided into two classes using a radiance threshold of 0.1 nW. Those background grid cells with radiance

0.1 nW or higher are concentrated around lighting features, indicating that these are associated with atmospheric scatter, commonly referred to as glow. The third background class is the largest in terms of grid cell numbers, representing normal background largely free of biomass burning and glow.

Figure 13 shows the results from the Landscan analysis, with Landscan population count on the x axis and grid cell count on the y axis. Note that a log scale is used on the y axis to accommodate the wide range of values. The large data cloud is from the VNL product, showing population counts where lighting was detected. The curves on the left are the fit lines for the three varieties of background: outlier removed, glow, and normal background. The triangle marks the grid cell counts for normal background having population count of zero. This group represents 98.7% of the normal background. The outlier removed grid cells had the lowest population counts of the three varieties of background and the glow has only a slight increase in population count when compared to the normal background. These results indicate that the outlier removal process is not removing population centres from the night-time lights product. Similarly, the glow

assigned to background falls outside of population centres and is nearly identical to the normal background lacking glow. Our conclusion is that the outlier, glow, and background removal are working as intended.

Figure 13. Comparison of Landscan population counts from four sets of grid cells in Australia. The data points are from the VIIRS night-time lights. The three trend lines show results from three varieties of background. ORM refers to grid cells where the average of high end outliers was 5 nW or more. GLOW are background grid cells where the average radiance was 0.1 nW and higher, BKG is the remainder of the background grid cells after removal of ORM and GLOW.

Display full size

4. Discussion

The VNL product indicates the locations and brightness of human settlements, from large cities down to small towns and many exurban housing clusters. Many bright linear road features propagate into the VNL product, but

dimmer road features are frequently missed. There is a narrow ring of grid cells surrounding each feature that probably has no detectable surface lighting but exceeds the data range threshold used to select the local background.

The quality of the VIIRS night-time lights product banks on two principals. The first is that the quality of the data product can be improved by excluding data featuring signal from phenomena other than electric lighting. This includes sunlit, moonlit, and cloudy pixels. The other principal that enhances the quality of the product is the 'power of the mean.' That is to say, the stability of the average night-time lights radiance improves through the inclusion of larger numbers of observations. For example, there are scan angle effects on the brightness of lights. These effects tend to cancel out through the averaging of radiances from all available scan angles. Another example is the seasonal effects on the observed radiances, which tends to cancel out through the inclusion of observations across multiple seasons.

The night-time VCM is rated to have a global cloud omission rate of 7.3% (Kopp et al. 2014). Thus, the cloud-free composite is corrupted by

the inclusion of approximately 7% cloudy observations that are incorrectly marked as clear. Opaque clouds will block the detection of lights at the Earth's surface. Thinner clouds will reduce the observed radiance and blur the spatial features. It appears that the outlier removal process works to remove pixels whose radiances have dimmed as a result of undetected clouds. For those cloud impacted pixels which pass through the outlier removal, the product again banks on the 'power of the mean' to arrive at a stable average through the inclusion of large numbers of observations.

The 2015 VNL product can be analysed to identify the brightest spot on Earth. This is often thought to be Las Vegas, Nevada, home of extraordinary casino lighting, including the 273,000 W sky beacon shining up from the Luxor hotel casino. Indeed, the brightest spot in Las Vegas has an average radiance of 2800 nW, marking it as the brightest urban area in the world. However, the Las Vegas radiance is dwarfed by the average radiance recorded at many gas flares. Close inspection reveals the brightest spot on Earth to be a gas flare in Venezuela, tipping out at 97,892 nW. Worldwide, large gas flares clearly exceed the brightness of human settlements. While most

electric lights have shielding and adhere to local regulations on lighting intensity, gas flares are under no such constraints and represent the worst offenders to dark skies. Figure 14 shows the glow extending around the bright gas flares in Venezuela.

Figure 14. Glow surrounding the brightest cluster of gas flares in 2015, located near Madrid, Venezuela. The red spots indicate average radiances over 10,000 nW cm^{-2} sr^{-1}. These are the gas flare locations.

Display full size

5. Conclusion

Satellite-observed global night-time lights indicate locations and brightness of light that escapes to space. Only specialized low-light imaging sensors are capable of acquiring the source data for night-time lights. Having mid-to-longwave infrared data collected simultaneously is an important asset, enabling cloud screening. For global product generation, there needs to be dozens of observations per year to have sufficient observations to filter out

extraneous features unrelated to surface lighting. From the mid-1970s to 2011, the only instrument meeting these criteria was the US Air Force DMSP OLS, which collected a complete set of night-time images of the Earth every 24 h. NOAA made a time series of annual global night-time lights product with OLS data spanning 1992–2013. While the OLS products have been widely utilized by scientists and economists, the OLS data have several flaws, including a dynamic range limited by six-bit quantization, coarse spatial resolution, and no in-flight calibration. Under normal operating conditions, the OLS saturates on bright urban cores. In 2011, NASA and NOAA launched the SNPP satellite, carrying the VIIRS, which collects low-light imaging data with 14 bit quantization, lower detection limits, wider dynamic range and 45 times smaller pixel footprints when compared to the OLS. As with the OLS, VIIRS collects a complete set of night-time images of the Earth every 24 h. In this article, we have outlined the basic set of steps involved in making an annual night-time lights product from VIIRS data.

Any instrument that has detection limits low enough to detect electric lighting present at the Earth's surface will also detect a set of

phenomena that are unrelated to surface lighting, including traces of reflected sunlight, stray light, lightning, aurora, biomass burning, and HEPs. Under moonlit conditions, the array of extraneous features expands to clouds, snow, and lunar glint. To make a research quality night-time lights product from VIIRS data requires a cascading series of filtering steps to strip out data contaminated by extraneous features prior to temporal averaging. This filtering is essential to producing a highly uniform standardized night-time lights product. Solar zenith angle thresholds are used to filter out sunlit and stray light contaminated data. The satellite zenith angle for each pixel is provided in the VIIRS geolocation file. A lunar illuminance threshold is used to filter out moonlit data. We developed specialized algorithms to identify and exclude pixels contaminated by lightning and HEP detections. More than a decade ago, we developed an outlier removal algorithm to filter fires from OLS composites. This was revised to work with VIIRS data and effectively removes biomass burning and other temporal lights to produce an ORCFC. With the OLS data, background was identified with manually drawn vectors. For VIIRS, we developed a set of

procedures to identify background pixel sets based on low data range (maximum minus minimum) and lack of expression for dim human settlements. The result is a grid of background seed radiances where areas with or adjacent to surface lighting have null (zero) values. The surface lighting holes are filled with the radiance of the nearest seed radiance. A delta is applied to the background to reduce false detections of surface lighting in areas having low numbers of cloud-free observations. Grid cells with positive radiances following the subtraction of the background (plus delta) from the ORCFC are deemed to have surface lighting present. The night-time lights product reports the ORCFC average radiance for the grid cells deemed to have surface lighting.

The current VNL product represents a major advance over the previous monthly DNB RCFCs. In addition to electric lighting, the RCFC products record lighting from biomass burning, aurora, and high albedo surfaces such as high-altitude mountain tops. In addition, the monthly products invariably have data outages in heavily clouded areas and at high latitudes in the months surrounding the summer solstice. These effects have been fully removed from the 2015 VIIRS night-time lights product.

The primary remaining sets of features that are unrelated to electric lighting are gas flares, which for large flares create vast quantities of glow surrounding the flare sites. Gas flares are at the top of the list in terms of the brightest spots on Earth. For artificial sky brightness studies, the inclusion of the gas flares and surrounding glow is of great value. However, for urban studies, the flares and glow are distractions. We provide a 2015 gas flare vector set as a guide to researchers.

There are several reasons for processing night-time lights using full years of data. Global night-time lights products require data from winter seasons to obtain usable CVGs at mid-to-high latitudes. Processing a full year of data ensures that the winter seasons are covered for both northern and southern hemispheres. Observations obtained during the dry season are particularly valuable for night-time lights. Dry seasons typically occur over several months, but the specific months are variable. Inclusion of a full year of data helps ensure that the local dry season is covered. Having large numbers of cloud-free observations is key to successful outlier removal, key to removal of biomass burning. All of these reasons point towards annual increments for the production

of research quality night-time lights.

Future plans for improvement of the VNL grids
include algorithm development to better filter
out the glow surround flares and large cities.
Research is ongoing on methods for extraction
of dimly lit roadways that can be observed
visually but are lost in the final step going from
ORCFC to VNL. Other areas for improvement of
the product include a background subtraction
and an atmospheric correction.

Disclosure statement

No potential conflict of interest was reported by
the authors.

Additional information

Funding

References

1. Amaral, S., G. Camara, A. M. V. Monteiro, J. A. Quintanilha, and C. D. Elvidge. 2005. "Estimating Population and Energy Consumption in Brazilian Amazonia Using DMSP Night-Time Satellite Data." *Computers, Environment and Urban Systems* 29 (2): 179–195. doi:10.1016/j.compenvurbsys.2003.09.004. [Crossref], [Google Scholar]

2. Baugh, K., C. D. Elvidge, T. Ghosh, and D. Ziskin. 2010. "Development of a 2009 Stable Lights Product Using DMSP/OLS Data." *Proceedings of the Asia Pacific Advanced Network* 30: 114–130. doi:10.7125/APAN.30.17. [Crossref], [Google Scholar]

3. Bharti, N., A. J. Tatem, M. J. Ferrari, R. F. Grais, A. Djibo, and B. T. Grenfell. 2009. "Explaining Seasonal Fluctuations of Measles in Niger Using Nighttime Lights Imagery." *Science* 334 (6061): 1424–1427. doi:10.1126/science.1210554. [Crossref], [Web of Science ®], [Google Scholar]

4. Bright, E. A., A. N. Rose, and M. L. Urban,

2016. Landscan 2015 High-Resolution Global Population Data Set. Report published by Oak Ridge National Laboratory, Oak Ridge, TN, USA. [Google Scholar]

5. Chand, K., K. V. S. Badarinath, C. D. Elvidge, and B. T. Tuttle. 2009. "Spatial Characterization of Electrical Power Consumption Patterns over India Using Temporal DMSP-OLS Night-Time Satellite Data." *International Journal of Remote Sensing* 30: 647–661. doi:10.1080/01431160802345685. [Taylor & Francis Online], [Web of Science ®] , [Google Scholar]

6. Elvidge, C. D., K. Baugh, M. Zhizhin, and F. C. Hsu. 2013 January 13-18. "Why VIIRS Data are Superior to DMSP for Mapping Nighttime Lights. *Proceedings of the Asia-Pacific Advanced Network*." In *Asia-Pacific Advanced Network*, edited by C. Elvidge, 62–69. USA: East-West Center, University of Hawai'i - Manoa. [Google Scholar]

7. Elvidge, C. D., M. Zhizhin, K. Baugh, and F. C. Hsu. 2015. "Automatic Boat Identification System for VIIRS Low Light Imaging Data."

Remote Sensing 7: 3020–3036.
doi:10.3390/rs70303020.
[Crossref], [Web of Science ®],
[Google Scholar]

8. Elvidge, C. D., M. Zhizhin, K. Baugh, F. C. Hsu,
    and T. Ghosh. 2016. "Methods for Global
    Survey of Natural Gas Flaring from Visible
    Infrared Imaging Radiometer Suite Data."
    Energies 9 (1): 14. doi:10.3390/en9010014.
    [Crossref], [Web of Science ®],
    [Google Scholar]

9. Falchi, F., P. Cinzano, D. Duriscoe, C. C. M.
    Kyba, C. D. Elvidge, and K. Baugh. 2016. "The
    New World Atlas of Artificial Night Sky
    Brightness." *Science Advances* 2 (6):
    e1600377. doi:10.1126/sciadv.1600377.
    [Crossref], [PubMed], [Web of Science ®],
    [Google Scholar]

10. Frangi, A. F., W. Niessen, K. Vincken, and M.
    Viergever. 1998. "Multiscale Vessel
    Enhancement Filtering." *Medical Image
    Computing and Computer-Assisted
    Intervention — MICCAI'98 Lecture Notes in
    Computer Science* 130–137.
    doi:10.1007/bfb0056195. [Crossref],

[Google Scholar]

11. Ghosh, H. T., R. Powell, C. D. Elvidge, K. E.
     Baugh, P. C. Sutton, and S. Anderson. 2010.
     "Shedding Light on the Global Distribution of
     Economic Activity." *Open Geography Journal*
     3: 147–160.
     doi:10.2174/1874923201003010147.
     [Crossref], [Google Scholar]

12. Godin, R., and G. Vicente. 2015. *Joint Polar
     Satellite System (JPSS) Operational Algorithm
     Description (OAD) Document for VIIRS Cloud
     Mask (VCM) Intermediate Product (IP)
     Software, National Aeronautics and Space
     Administration (NASA)*. Greenbelt, Maryland:
     Goddard Space Flight Center. Doi:accessed
     on 12th April 2017. Available online at:
     https://jointmission.gsfc.nasa.gov/sciencedocs/2015-
     08/474-00062_OAD-VIIRS-Cloud-Mask-
     IP_I.pdf [Google Scholar]

13. He, C., Q. Ma, T. Li, Y. Yang, and Z. Liu. 2012.
     "Spatiotemporal Dynamics of Electric Power
     Consumption in Chinese Mainland from 1995
     to 2008 Modeled Using DMSP/OLS Stable
     Nighttime Lights Data." *Journal of
     Geophysical Sciences* 22 (1): 125–136.

[Google Scholar]

14. Janiczek, P. M., and J. A. Deyoung. 1987.
    Computer Programs for Sun and Moon
    Illuminance with Contingent Tables and
    Diagrams. U.S. Naval Observatory Circular
    171. Doi:accessed on 12th April 2017.
    Washington, DC: U.S. Naval Observatory.
    Available online at:
    http://aa.usno.navy.mil/publications/docs/Circular_171.pdf
    [Crossref], [Google Scholar]

15. Kopp, T. J., W. M. Thomas, A. K. Heidinger, D.
    Botambekov, R. A. Frey, K. D. Hutchinson, B.
    D. Lisager, K. Brueske, and B. Reed. 2014.
    "The VIIRS Cloud Mask: Progress in the First
    Year of S-NPP toward a Common Cloud
    Detection Scheme." *Journal of Geophysical*
    Research – Atmospheres 119: 2441–2456.
    doi:10.1002/2013JD020458.
    [Crossref], [Web of Science ®],
    [Google Scholar]

16. Lindeberg, T. 1998. "Feature Detection with
    Automatic Scale Selection." *International*
    Journal of Computer Vision 30 (2): 79–116.
    doi:10.1023/A:1008045108935.
    [Crossref], [Web of Science ®],

[Google Scholar]

17. Mazor, T., N. Levin, H. P. Possingham, Y. Levy, D. Rocchini, A. J. Richardson, and S. Kark. 2013. "Can Satellite-Based Night Lights Be Used for Conservation? The Case of Nesting Sea Turtles in the Mediterranean." *Biological Conservation* 159: 63–72. doi:10.1016/j.biocon.2012.11.004. [Crossref], [Web of Science ®], [Google Scholar]

18. Miller, S. D., S. P. Mills, C. D. Elvidge, D. T. Lindsey, T. F. Lee, and S. J. D. Hawkin. 2012. "Suomi Satellite Brings to Light a Unique Frontier of Environmental Sensing Capabilities." *Proceedings of the National Academy of Sciences of the United States of America* 109 (39): 15706–15711. doi:10.1073/pnas.1207034109. [Crossref], [PubMed], [Web of Science ®], [Google Scholar]

19. Miller, S. D., W. Straka III, S. P. Mills, C. D. Elvidge, T. F. Lee, J. Solbrig, A. Walther, A. K. Heidinger, and S. C. Weiss. 2013. "Illuminating the Capabilities of the Suomi NPP VIIRS Day/Night Band." *Remote Sensing*

5 (12): 6717–6766. doi:10.3390/rs5126717.
[Crossref], [Web of Science ®],
[Google Scholar]

20. Mills, S., S. Weiss, and C. Liang. 2013. "VIIRS
     Day/Night Band (DNB) Stray Light
     Characterization and Correction."
     *Proceedings SPIE 8866, Earth Observing
     Systems XVIII,* 88661P. [Crossref],
     [Google Scholar]

21. Min, B., K. Gaba, O. F. Sarr, and A. Agalassou.
     2013. "Detection of Rural Electrification in
     Africa Using DMSP-OLS Night Lights
     Imagery." *International Journal of Remote
     Sensing* 34 (22): 8118–8141.
     doi:10.1080/01431161.2013.833358.
     [Taylor & Francis Online], [Web of Science ®]
     , [Google Scholar]

22. Oda, T., and S. Maksyutov. 2011. "A Very
     High-Resolution (1 Km×1 Km) Global Fossil
     Fuel CO_2 Emission Inventory Derived Using a
     Point Source Database and Satellite
     Observations of Nighttime Lights."
     Atmospheric Chemistry and Physics 11:
     543–556. doi:10.5194/acp-11-543-2011.
     [Crossref], [Web of Science ®],

[Google Scholar]

23. Small, C., F. Pozzi, and C. D. Elvidge. 2005. "Spatial Analysis of Global Urban Extent from DMSP-OLS Night Lights." *Remote Sensing of Environment* 96: 277–291. doi:10.1016/j.rse.2005.02.002. [Crossref], [Web of Science ®], [Google Scholar]

24. Sutton, P. C., D. Roberts, C. D. Elvidge, and K. E. Baugh. 2007. "Census from Heaven: An Estimate of Global Human Population Using Nighttime Satellite Imagery." *International Journal of Remote Sensing* 22 (16): 3061–3076. doi:10.1080/01431160010007015. [Taylor & Francis Online], [Web of Science ®] , [Google Scholar]

25. Witmer, F. D. W., and J. O'loughlin. 2011. "Detecting the Effects of Wars in the Caucasus Regions of Russia and Georgia Using Radiometrically Normalized DMSP-OLS Nighttime Lights Imagery." *Giscience and Remote Sensing* 48 (4): 478–500. doi:10.2747/1548-1603.48.4.478. [Taylor & Francis Online], [Web of Science ®]

, [Google Scholar]

Information for

Authors

Editors

Librarians

Societies

Open access

Overview

Open journals

Open Select

Cogent OA

Dove Medical Press

F1000Research

Help and info

Help & contact

Newsroom

Commercial services

Advertising information

All journals

Books

Keep up to date

Register to receive personalised research and resources by email

Sign me up